20G/316L 双金属复合管弧焊接头组织与性能

吕世雄, 王 廷, 冯吉才
(哈尔滨工业大学 现代焊接生产技术国家重点实验室, 150001)

吕世雄

摘 要: 对 20G 内衬 316L 复合管进行了 TIG 焊对接试验, 并对接头进行了拉伸、弯曲、冲击、压力测试以及无损探伤, 利用光学、扫描电子显微镜以及化学分析方法对接头组织和主要合金元素的扩散进行了分析. 结果表明, 焊缝分为碳钢层、碳钢与过渡层间的扩散层、过渡层和不锈钢层四个区域. 扩散层焊缝组织为马氏体+残余奥氏体, 过渡层为奥氏体组织, 而不锈钢层则为胞状树枝晶. 在试验参数下, 接头各项力学性能优良, 接头无缺陷. 焊缝根部 Ni, Cr 合金元素与焊接材料相比无明显变化, 采用过渡焊丝起到了保持根部焊缝合金元素含量的作用.

关键词: 20G/316L 复合管; TIG 焊; 显微组织; 力学性能
中图分类号: TG444+.74 文献标识码: A 文章编号: 0253-360X(2009)04-0093-04

0 序 言

随着石油、天然气开采规模的扩大, 经常需要跨地域的长距离的管道输送. 碳钢管的耐腐蚀性能较差, 经常发生泄漏事故. 若采用不锈钢管进行输送, 则会极大地提高运输成本, 因此近年来, 碳钢内衬不锈钢管的双金属复合管由于其优良的耐腐蚀性能以及相对较低的成本, 在炼油、石化、化工、电力、冶金、医药以及食品加工等领域逐步推广使用[1,2]. 由于双金属复合管本身的特殊性尚无很成熟的焊接工艺, 焊接时容易在衬层与基体的界面处出现未熔合缺陷. 同时基层碳钢中的碳元素向不锈钢中的扩散会降低不锈钢内衬的抗腐蚀性能[3-5]. 目前对于复合管焊接的研究主要集中于焊接工艺, 对 20G/316L 复合管进行了焊接试验, 针对复合管焊接的难点, 提出新的焊接工艺, 同时对焊接接头显微组织进行了详细分析, 解释了焊接试验工艺的可行性.

1 试验材料

1.1 复合管材料

试验材料为 316L 与 20G 复合管, 规格为 ϕ76 mm×(7+2) mm. 基材采用常用的 20G 材质, 复合层为 316L 奥氏体不锈钢. 试验材料化学成分见表 1, 力学性能见表 2.

收稿日期: 2008-03-18

表 1 材料化学成分(质量分数, %)

Table 1 Chemical composition of materials

	C	Mn	Si	S	P	Cr	Ni	Cu	Mo	Fe
316L	0.025	0.95	0.55	0.009	0.031	10.13	16.36	—	2.00	余量
20G	0.19	0.52	0.31	0.013	0.024	—	—	0.2	—	余量

表 2 材料力学性能

Table 2 Mechanial properties of pipe materials

	屈服强度 R_{eL}/MPa	抗拉强度 R_m/MPa	断后伸长率 A(%)
316L	255	600	63
20G	300	485	29.5

1.2 焊接材料

对于复合层不锈钢焊接, 试验选用与母材成分相近的 ϕ1.2 mm HS316L 焊丝. 基层选用焊丝为 ϕ1.2 mm ER55-G, 为了防止碳层材料对基层不锈钢材料的稀释以及碳元素的扩散, 在基层与复合层之间添加镍铬含量较高的过渡焊丝, 试验选用规格为 ϕ1.2 mm 的 ER309L. 各种焊丝化学成分见表 3.

表 3 焊丝化学成分(质量分数, %)

Table 3 Composition of welding wires

	C	Mn	Si	S	P	Cr	Ni	Mo	其它
HS316L	0.024	1.57	0.65	0.001	0.015	18.37	11.36	2.10	余量
ER55-G	0.084	1.31	0.81	0.006	0.009	1.24	—	0.63	余量
ER309L	0.025	2.04	0.51	0.006	0.023	23.43	13.43	0.03	余量

2 焊接工艺及过程

2.1 坡口设计及气体保护装置

复合管焊接的难点在于如何避免基层低碳钢对不锈钢的稀释从而避免不锈钢焊缝耐腐蚀性的下降,为此采用图 1a 所示的坡口设计,打底焊在“裸露”出来的不锈钢上进行. 焊道设计及焊接顺序如图 1b 所示. 焊接时需要背部气体保护,保护装置如图 2 所示,采用两橡胶挡板置于焊缝两侧,构成封闭氩气仓,实现了对管内的保护.

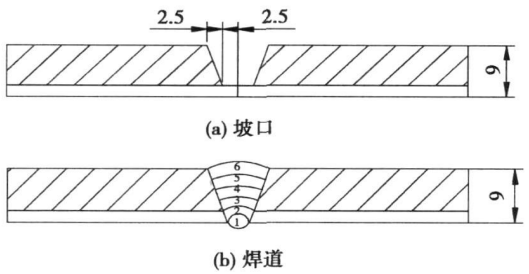

图 1 坡口及焊道设计(mm)

Fig. 1 Schematic figures of groove and bead design

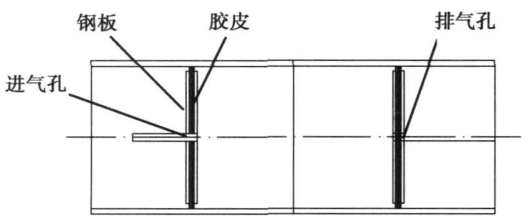

图 2 氩气内保护装置示意图

Fig. 2 Schematic diagram of Ar inner protection

2.2 焊接方法及参数

为了缩短焊接时高温停留时间,复合层焊接时,选用热输入较小的脉冲 TIG 焊接方法. 为了保证充分的熔合,过渡层和基层焊接采用直流 TIG 焊. 复合层焊接参数见表4. 过渡层和基层的焊接参数见表 5. 试验中层间温度控制在 70~80 ℃.

表 4 复合层焊接参数

Table 4 Welding parameters of composite bead

焊道	电源极性	脉冲电流 I_b/A	基值电流 I_b/A	脉宽比 λ(%)	脉冲频率 f/Hz	气体流量 q/(L·min^{-1}) 正面	气体流量 背面	焊接速度 v_1/(m·min^{-1})	送丝速度 v_2/(m·min^{-1})
1	DC−	100	45	50	2	10	12	0.18	0.4~0.5
2	DC−	140	70	50	2	10	12	0.18	0.5~0.6

注: DC− 表示钨极接负

表 5 过渡层和基层的焊接参数

Table 5 Welding parameters of transition and base beads

焊道	电源极性	焊接电流 I/A	气体流量 q/(L·min^{-1})	送丝速度 v_1/(m·min^{-1})	焊接速度 v_2/(m·min^{-1})
3~6	DC−	160	12	0.8~1.0	0.18

3 试验结果与分析

3.1 力学性能测试

为了评定焊接工艺,对接头抗拉强度、抗弯强度以及常温冲击性能进行了测试,结果见表 6.

表 6 焊接接头力学性能

Table 6 Mechanical properties of welding joints

抗拉强度 R_m/MPa	断后伸长率 A(%)	断裂位置	抗弯强度 R_w/MPa	弯曲角度 θ/(°)	冲击吸收功 A_{KV}/J
516	21	母材	996	150	63

水压试验破坏压力可达 14 kN,裂口出现在母材上. 依据国家标准 GB/T3323—2005,对焊缝进行了 X 射线探伤,焊缝无缺陷,达到 I 级焊缝水平.

3.2 接头显微组织分析

图 3 为焊缝的宏观形貌,由图可看出,焊缝可以明显地分为碳钢层、碳钢与过渡层间的扩散层、过渡层和不锈钢层四个区域.

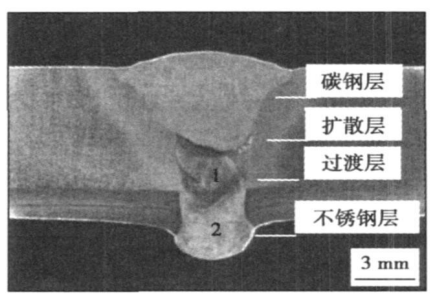

图 3 焊缝整体形貌

Fig. 3 Macrosturcture of weld

图 4 为扩散层显微组织,由于过渡层与碳钢层焊接材料成分差异较大,在这两层之间出现明显的元素扩散层,该区由于合金化元素 Ni, Cr 等含量增加,组织基本为细小的马氏体+部分残余奥氏体. 图 5 为过渡层焊缝区组织,过渡层由于合金化元素含量高,为类固溶体的奥氏体,组织更加细小.

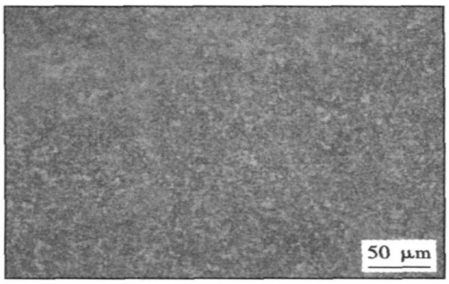

图 4　扩散层焊缝显微组织

Fig. 4　Microstructure of diffusion layer weld

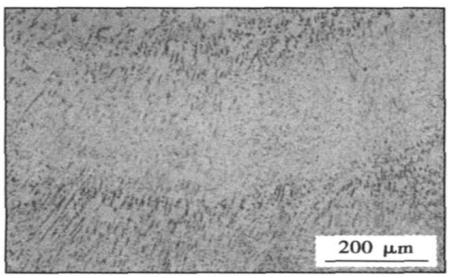

图 5　过渡层焊缝显微组织

Fig. 5　Microstructure of transition layer weld

图 6 为不锈钢层接头热影响区组织，主要为奥氏体＋δ铁素体．由于碳含量低，故没有发生明显的晶粒长大．图 7 为不锈钢层焊缝组织，主要为胞状树枝晶．

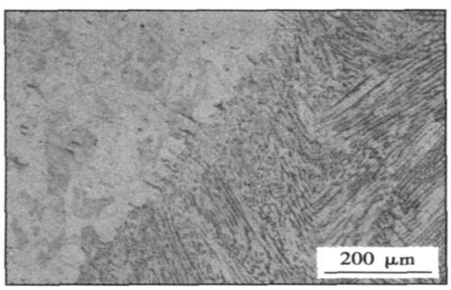

图 6　不锈钢层接头热影响区组织

Fig. 6　Microstructure in HAZ of stainless steel joint

3.3　合金元素的扩散

由于复合管接头中基层及所用焊接材料与不锈钢复合层化学成分差异较大，故存在不锈钢中合金元素向碳钢以及碳钢中碳元素向不锈钢的扩散．对图 3 中位置 1 和 2 进行了能谱分析，表 7 为主要合金元素在过渡层和不锈钢层以及对应焊接材料中含量的比较．可以看出在过渡层熔化区内，与对应焊接材料相比合金元素的含量降低，而在不锈钢层熔化区内，与对应焊接材料相比合金元素含量没有发生明显变化．说明基层碳钢对过渡层合金元素有明显的稀释作用，而过渡层对复合层不锈钢层焊缝起到了很好的隔离作用，从而保持了不锈钢层焊缝中的合金元素含量，有助于提高焊缝的耐腐蚀性能．

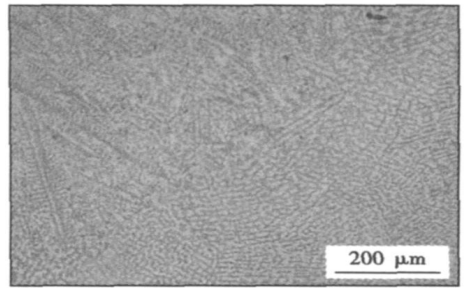

图 7　不锈钢层焊缝显微组织

Fig. 7　Microstructure of stainless stee weld

表 7　过渡层和不锈钢层焊缝与对应焊接材料中合金元素含量(质量分数，%)

Table 7　Composition of alloying elements in transition and stainless steel weld

材料	Mo	Cr	Ni	Mn
过渡层焊缝	2.14	13.52	8.51	—
过渡层焊丝	2.34	23.43	13.43	0.03
不锈钢层焊缝	2.13	16.84	10.33	1.16
不锈钢焊丝	2.10	18.37	11.36	1.57

表 8 为焊缝底部与不同层焊接材料及基层碳钢中碳元素含量的对比，可以看出焊缝底部碳含量低于 0.1%，从而有利于不锈钢焊缝耐腐蚀性能的保持．从表中还可以看出，焊缝底部碳元素含量高于不锈钢层和过渡层焊丝中的碳含量，而远远小于基层碳钢中的含碳量，说明过渡层起到了隔离作用，这是因为过渡层中碳化物形成元素铬含量较高，降低了碳的活度，从而阻碍了其向不锈钢层焊缝中的扩散．从图 3 可以看出，复合层不锈钢与基层碳钢发生了一定的互溶，说明这一部位为碳元素扩散迁移的主要通道，该过程也应为控制焊缝底部含碳量的主要步骤．

表 8　焊缝底部与不同焊接材料与母材中的碳元素含量(质量分数，%)

Table 8　Composition of carbon element in weld root and welding materials

316L	20G	HS316L	ER309L	焊缝底部
0.025	0.19	0.024	0.025	0.058

3.4 接头硬度分布

图 8 为碳钢层沿水平方向的硬度分布，原点处表示焊缝中心位置. 可以看出在熔合线附近硬度最高，这是因为在该部位存在渗碳层的缘故，焊缝各区域的硬度均高于母材，从而保证足够高的接头强度. 图 9 为碳钢层沿焊缝纵向中心线的硬度分布，原点表示焊缝底部起始位置，在过渡层及扩散层硬度最高，该区域合金元素含量高，形成马氏体组织，提高了焊缝的强韧度. 图 10 为沿不锈钢层焊缝水平方向的硬度分布，原点同样为焊缝中线位置，硬度在该方向基本呈水平，说明焊缝在热作用下组织性能与母材相比没有明显变化，都为奥氏体组织. 也说明没有碳含量明显增加的区域存在.

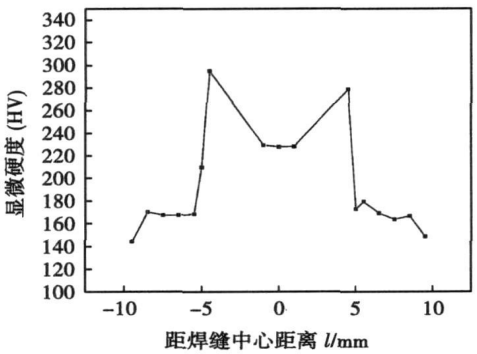

图 8 碳钢层沿水平方向的硬度分布

Fig. 8 Horizontal microhardness distribution of carbon steel joint

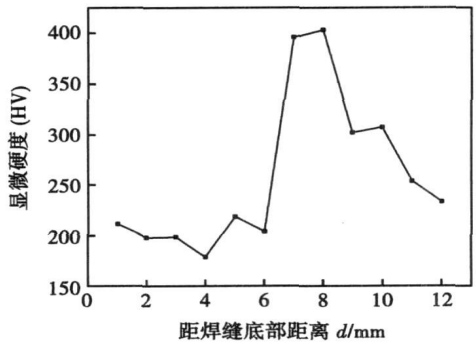

图 9 碳钢层沿焊缝纵向中心线的硬度分布

Fig. 9 Vertical microhardness distribution of carbon steel joint

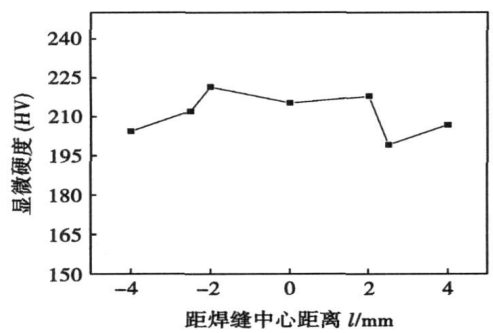

图 10 不锈钢层焊缝沿水平方向的硬度分布

Fig. 10 Horizontal microhardness distribution of stainless steel joint

4 结 论

(1) 采用试验中的焊接工艺可以得到力学性能优良的复合管焊接接头.

(2) 过渡层金属中合金元素被碳钢稀释，而不锈钢焊缝金属中合金元素含量没有明显降低，过渡层起到了良好的隔离作用.

参考文献：

[1] 齐敬春，王明鹏. 碳钢内衬不锈钢复合管材的特性及应用[J]. 中国建材科技，2005(3)：23－25.
Qi Jingchun, Wang Mingpeng. Characteristic and application of the pipe that carbon steel inside lining stainless steel compounds[J]. China Building Materials Scinece & Technology, 2005(3): 23－25.

[2] 於 方，秦建平. 双金属管在管道输送中的应用[J]. 钢管，2000，29(1)：34－36.
Yu Fang, Qin Jianping. Application of dual metal pipe in pipe line service[J]. Steel Pipe, 2000, 29(1): 34－36.

[3] 王能利，潘希德，薛 锦. 20/0Cr18Ni9 复合管焊接工艺和接头的抗腐蚀性能[J]. 焊接，2003(5)：23－26.
Wang Nengli, Pan Xide, Xue Jin. Welding procedure and resistant to corrosion properties for welded joint of 20/0Cr18Ni9 clad pipe[J]. Welding & Joining, 2003(5): 23－26.

[4] 李萌盛. 异质焊接接头加热过程中的碳迁移现象研究[J]. 材料科学与工艺，1997，5(3)：17－21.
Li Mengsheng. Carbon migration for dissimilar metal joints in heating process[J]. Materials Science & Technology, 1997, 5(3): 17－21.

[5] 史春元，李小刚，于启湛，等. 异种钢焊接接头加热后碳迁移区力学性能的变化规律[J]. 焊接学报，2000，21(3)：59－62.
Shi Chunyuan, Li Xiaogang, Yu Qizhan, *et al*. Mechanical properties of carbon migration zone of dissimilar steel welded joints after heating [J]. Transaction of the China Welding Institution, 2000, 21(3): 59－62.

作者简介：吕世雄，男，1957 年出生，博士，高级工程师. 主要从事有色金属焊接方面的科研工作. 发表论文 20 余篇.

Email：lvshixiong@hit.edu.cn

According to the welding heat input control based on the EN and EP transition, the arc instability and exclusion have been improved. In order to make the energy control continuous, double transition was implemented in each cycle. This method can control the energy during welding process with the heat distribution control of the base metal and wire. The welding machine designed for this method can meet the technical requirements and realize service reliability and precise output. The experimental results indicate the AC shortcircuit tansfer technique has stable welding with the less spatter and the good weld bead.

Key words: energy; welding; AC; shortcircuit transition

Microstructure and properties of transient liquid phase diffusion bonded joint for TiNi shape memory alloy and stainless steel

WANG Yingling[1], LI Hong[1], LI Zhuoxin[1,2], FENG Jicai[2] (1. College of Materials Science and Engineering, Beijing University of Technology, Beijing 100124, China; 2. State Key Lab of Advanced Welding Production Technology, Harbin Institute of Technology, Harbin 150001, China). p77—80

Abstract: TiNi shape memory alloy and stainless steel were bonded by transient liquid phase diffusion bonding (TLP-DB) with AgCu metal foil as the interlayer. The microstructure, alloy elements profile and the patterns of joint were analyzed, while the microhardness and the shear strength of the joint were investigated. The results show that the interface zone of joint is composed of TiNi transition zone, middle zone and stainless steel transition zone, which contains Ti(Cu, Ni, Fe) phase, AgCu phase, TiFe phase respectively. The microhardness of diffusion zone in both TiNi side and stainless steel side wries in the range of 500-650 HV. However, the microhardness of middle zone is only about 120 HV. With the increase of heating temperature or the prolonging of the holding time, the shear strength of joint interface increases firstly and then decreases. The highest shear strength is about 239.4 MPa. The fracture occurs at diffusion interface between TiNi alloy and AgCu interlayer, and the joint presents a characteristic of mixed fracture ductile-brittle mode.

Key words: TiNi shape memory alloy; stainless steel; transient liquid phase diffusion bonding; microstructure; shear strength

Residual stress evaluation of high-speed train body structure by ultrasonic method and verification

LU Hao[1], LIU Xuesong[1], MENG Lichun[2], MA Ziqi[1], FANG Hongyuan[1] (1. State Key Laboratory of Advanced Welding Production Technology, Harbin Institute of Technology, Harbin 15001, China; 2. CSR Sifang Locomotive and Rolling Stock. Co. Lt, Qingdao 266000, Shandong, China). p81—83

Abstract: Residual stress is one of the most important challenges to the safety of parts and structures as welled. Ultrasonic stress measurement system is modified for the measurement of thin wall welded structure. The residual stress of high-speed train body structure is measured by the system. The measurement process is not only nondestructive, but also real-time and quick. The results of the ultrasonic method are verified by the laser hologram interference hole-drilling method and finite element method. The deviations of the results are also discussed.

Key words: ultrasonic; thin wall welded structure residual stress; high-speed train; nondestructive

Fabrication and property of nano-SiC whisker/ZrO_2 composite thermal barrier coatings

HOU Pingjun, WANG Hangong, WANG Liuying, ZHA Bailin (The Second Artillery Engineering College 501 staff, Xi'an 710025, China). p84—88

Abstract: SiC whisker (SiC_w)/ZrO_2 composite thermal barrier coatings (CTBCs) were sprayed by micro-plasma on stainless steel substrates. Both nano-ZrO_2 and micro-ZrO_2 were used in the CTBCs. The zirconia powders were 7 wt% Y_2O_3 partially stabilized ZrO_2 (YPSZ). Microstructure of the coatings was analyzed by scanning electron microscopy (SEM). The chemical composition of the top coating was measured by energy dispersive X-ray (EDX). Phase content of the coatings investigated by X-ray diffraction (XRD). In the spraying process, a large quantity of SiC_w in the powder has been decomposed at high temperature, which produces pores in the top coating, and little SiC_w embedded in the top coating decreases the thermal stress, nailing and bridging the coating. With SiC_w content increasing, the porosity of composite TBCs was increased, and the thermal shock life was improved firstly and weakened later. The highest thermal shock resistance was achieved at 20% volume ratio of SiC_w to nano-ZrO_2, was better than that of the single ZrO_2 coatings.

Key words: thermal barrier coatings (TBCs); micro-plasma spray; SiC whisker; composite coating; thermal shock resistant

Study on cold cracking susceptibility of domestic X80 pipeline steel using implant tests

HUANG Fuxiang[1,2], DU Zeyu[1], SUI Yongli[2], ZENG Huilin[1,2], GUO Xiaojiang[2] (1. School of Materials Science and Engineering, Tianjin University, Tianjin 300072, China; 2. Pipeline Research Institute of CNPC, Langfang 065001, Hebei, China). p89—92

Abstract: Cold crack sensitivity and the fracture characteristic of the root pass welding of X80 pipeline steel CO_2 gas shielded arc weld with solid wire was investrgated by implant testing. The results indicate that the X80 steel has the excellent resistance to cold cracking under the preheating 100 ℃ condition, the critical breaking stress σ_{cr} (624 MPa) is equivalent to its tensile strength Rm. When the tension stress is higher than Rm, the expiration break would happen, and the breaking nature is the ductile fracture. Under the condition of CO_2 gas shielded arc weld for root pass, the good resistence to crack characteristic of X80 steel has not only been related with the welding procedure with the ultra low hydrogen welding, but also with the lower crack sensitive coefficient (0.17%) as well as the unobvious quench hardening of HAZ. The microstructure of superheat section, with the maximum hardness degree of 297 HV is mainly the block ferrite.

Key words: X80 pipeline steel; implant test; cold crack; root weld

Microstructure and mechanical properties of TIG welded 20G/316L clad pipe joint

LV Shixiong, WANG Ting, FENG Jicai

(State Key Laboratory of Advanced Welding Production Technology, Harbin Institute of Technology, Harbin 150001, China). p93—96

Abstract: Tensile strength, bending strength, impact toughness and non-destructive inspection tests of TIG welded 20G/316L clad pipe joint were carried out. The microstructure and the diffusion of the major alloying elements were analysed using optical microscopy, SEM and chemical analysis. The results showed that the weld can be divided into four layers including carbon steel layer, diffusion layer, transition layer and stainless steel layer. The microstructure in diffusion layer was characterized by the martensite and retained austenite. The transition layer only contained austenite, and the stainless steel layer included afterbirth-like crystal. The defect-free joint was produced and performed well under the experimental parameters. The concentration of nickel and chromium element in weld root did not decrease compared with the corresponding welding materials, which proved that the employment of transition welding wire could maintain the concentration of the major alloying elements in welding root.

Key words: 20G/316L clad pipe; TIG; microstructure; mechanical properties

Quality evaluation of the resistance spot welding based on PCA-SVM ZHANG Hongjie[1], HOU Yanyan[2] (1. School of Machinery and Electron, Tianjin Polytechnic University, Tianjin 300160, China; 2. Department of Architecture Engineering, Hebei College of Administration, Shijiazhuang 050031, China). p97—100

Abstract: The electrode displacement and dynamic resistance signals of resistance spot welding process are collected synchronously. Through the time-domain analysis of electrode displacement signal in the welding process, nine characteristic parameters relating to weld quality are picked up to set up a set of data which characterizes the input samples, on the basis of the different phase of nugget forming marked by simultaneous dynamic resistance signal. The principal component analysis (PCA) to remove the self-correlation of input characteristics and realize dimensionality reduction is integrated with the conventional method of support vector machine(SVM), while the shear strength of welded spot was taken as the evaluation index of welded spot quality. The comparison of predicted results under PCA-SVM and conventional SVM by means of cross-validation test shows that PCA-SVM algorithm improves the generalization ability and the predicted accuracy of SVM method.

Key words: resistance spot welding; principal component analysis; support vector machine; regression analysis

Numerical simulation of the temperature field during resistance spot welding with rectangular electrode ZHANG Xiaoqi[1,2], XU Guocheng[1], WANG Chunsheng[1,3], WEN Jing[1] (1. School of Material Science and Engineering, Jilin University, Changchun 130025, China; 2. Jilin Teachers Institute of Rnqineeriy and Fechnology, Changchen 130052, China; 3. Changchun Railway Vehicles Corporation, Changchun 130062, China). p101—104

Abstract: The temperature field during resistance spot welding with rectangular electrode was simulated using ANSYS. The physical model was properly simplified on the basis of simulation accuracy and technological conditions. One-quarter three-dimensional finite element model during resistance spot welding was built in which the contact resistance was substituted by the electric resistivity. The results show that at the beginning of welding, the edge of electrodes has the highest temperature because of high stress induced by the electrode force. As welding time is longer, the contact resistance decreases and the highest temperature position moves to inside, the nugget appears to be similar with the conventional spot welding.

Key words: rectangular electrode; numerical simulation; temperature field

Laser-based visual recognition of multi-pass seam in robot arc welding ZHANG Huajun[1,2], ZHANG Guangjun[1], CAI Chunbo[2], GAO Hongming[1], WU Lin[1] (1. State Key Laboratory of Advanced Welding Production Technology, Harbin Institute of Technology, Harbin 150001, China; 2. College of Material Science and Engineering, Harbin University of Science and Technology, Harbin 150040, China). p105—108

Abstract: It is very necessary for the improvement of weld quality and the realization of robot automatic production to detect multi-pass weld profile parameters automatically. Automatic detective system of multi-pass weld profile parameters by band laser visual sensor was developed. The procedure of image process is as follows: smoothing, center recognition by longitudinal grey gradient, twice slope smooth process, and multiple peaks search by laser seam image analysis. It is very important for seam tracking, arc length control and torch attitude adjustment to obtain four character points of weld seam profile. And the recognition results agree with the experimental results.

Key words: multipass welding; laser visual sensor; image process; twice slope smooth process; robot arc welding

Research on gravity compensation algorithm for tool-assembling with force control in remote welding WEI Xiuquan, WU Lin, GAO Hongming, LI Haichao (State Key Laboratory of Advanced Welding Production Technology, Harbin Institute of Technology, Harbin 150001, China). p109—112

Abstract: Based on the control strategy of global teleoperative and local autonomous, a tool-assembling experimental system with force control for remote welding is established. The tool gravity calculation and linear least-squares algorithm are adopted to calibrate the tool load parameter, and a tool gravity compensation algorithm based on the tool load parameter vector is proposed to eliminate the gravity disturbance during the tool-assembling process with force control. For a customized assembing tool, experiments on load parameter calibration and gravity compensation in non-contact condition are carried out. The experimental results show that the tool gravity compensation algorithm can obtain a high precision, meeting the requirements of local autonomous force control in tool-assembing task, while the maximum error of gravity compensation and gravity moment compensation are 1 N and 0.1 N·m, respectively.

Key words: gravity compensation; force control; tool assembling; remote welding